TOP QUARK PHYSICS AT COLLIDERS* **

E.W.N. Glover

Institute for Particle Physics Phenomenology, University of Durham
Durham DH1 3LE, UK

F. del Águila, J.A. Aguilar–Saavedra, M. Beccaria, S. Béjar
A. Brandenburg, J. Fleischer, J. Guasch, T. Hahn, W. Hollik
S. Heinemeyer, S. Kraml, A. Leike, A. Lorca, W. Porod
S. Prelovsek, F.M. Renard, T. Riemann, C. Schappacher
Z.G. Si, J. Solà, P. Uwer, C. Verzegnassi, G. Weiglein
and A. Werthenbach

Universitat Autonoma de Barcelona, Universitat de Barcelona, CERN
Univ. of Durham, Univ.d de Granada, DESY, Hamburg, INFN Lecce
Univ. di Lecce, Instituto Superior Tecnico Lisbon, Univ. de Montpellier II
Ludwig-Maximilians-Univ. München, Max Planck Inst. für Phys. München
Shandong Univ., INFN Trieste, Univ. di Trieste, Paul Scherrer Institut Villigen
DESY, Zeuthen, Univ. Zürich, Universität Bielefeld

(Received October 11, 2004)

We review some recent developments in top quark production and decay at current and future colliders.

PACS numbers: 12.15.Lk, 12.38.Bx, 13.66.Bc, 14.65.Ha

1. Introduction

The detailed analysis of the dynamics of top quark production and decay is a major objective of experiments at the Tevatron, the LHC, and a possible international linear e^+e^- collider (ILC). A special feature of the top quark that makes such studies very attractive is its large decay width, $\Gamma_t \approx 1.48$ GeV, which serves as a cut-off for non-perturbative effects in top

* Presented by E.W.N. Glover at the final meeting of the European Network "Physics at Colliders", Montpellier, France, September 26–27, 2004.
** This work has been supported by the European Community's Human Potential Programme under contract HPRN-CT-2000-00149.

quark decays. As a consequence *precise* theoretical predictions of cross sections and differential distributions involving top quarks are possible within the Standard Model and its extensions. A confrontation of such predictions with forthcoming high-precision data will lead to accurate determinations of Standard Model parameters and possibly hints of new phenomena.

For more details on the general subject of top physics, we refer the reader to the recent collider studies [1–4] and references therein. In this talk, I review the joint contribution to top quark physics made by the network.

2. Top quark production at the ILC [5–9]

At the ILC, one of the most important reactions will be top-pair production well above the threshold (*i.e.* in the continuum region),

$$e^+ + e^- \to t + \bar{t}\,. \tag{1}$$

Several hundred thousand events are expected, and the anticipated accuracy of the corresponding theoretical predictions should be around a few per mille. Of course, it is not only the two-fermion production process (1), with electroweak (EW) and QCD radiative corrections to the final state that must be calculated with high precision. In addition, the decay of the top quarks and a variety of quite different radiative corrections such as real photonic bremsstrahlung and other non-factorizing contributions to six-fermion production and beamstrahlung have to be considered. New physics effects may also have to be taken into account.

In [10, 11], the complete $O(\alpha)$ corrections, including hard photon radiation, are calculated. The virtual and soft photon corrections both in the Standard Model (SM) and in the minimal supersymmetric Standard Model (MSSM) are determined in [12, 13], and (only) in the SM in [14]. At the time of the public presentation of the TESLA Technical Design Report [2]. detailed comparisons between these calculations had not been made. For this reason, and to produce an event generator for the evaluation of experimental data, the fortran code `topfit` has been written [5,6] which describes the fixed-order QED and electroweak one-loop corrections to top pair production.

Top quark pair production from e^+e^- annihilation at one-loop differs from light fermion production because two new structures appear in the theoretical description that are a consequence of the fact that the top mass is not negligible. To understand the origin of the extra structures, it is sufficient to consider the theoretical expansion of a one-loop vertex coupling the top quark pair to either a photon or a Z. In full generality, with

CP-conserving interactions one can identify the effective vertex [15]

$$\Gamma_\mu^X = -e^X \left[\gamma_\mu (g_{Vt}^X - g_{At}^X \gamma^5) + \frac{d^X}{m_t}(p - p')_\mu \right] \tag{2}$$

where $X = \gamma, Z$, $e^\gamma = |e|$, $e^Z = \frac{|e|}{2 s_W c_W}$ and p, p' represent the outgoing t, $\bar{t}$ momenta; g_{Vt}^X, g_{At}^X, d^X are $O(\alpha)$ one-loop contributions which in general are $q^2 = (p + p')^2$ dependent. The new quantity d^X enters because the top mass cannot be neglected and appear in the various theoretical expressions at one loop, making the overall number of independent amplitudes of the process to increase from four (in massless fermion production) to six. This is because the three independent coefficients of Eq. (2) will be combined with the two independent coefficients (g_{Vl}^X, g_{Al}^X) of the initial (massless) lepton current.

The one-loop corrections to $t\bar{t}$ production therefore consists of evaluating these six form factors. Typical one-loop vertex and box graphs contributing to the EW and QED corrections are shown in Fig. 1.

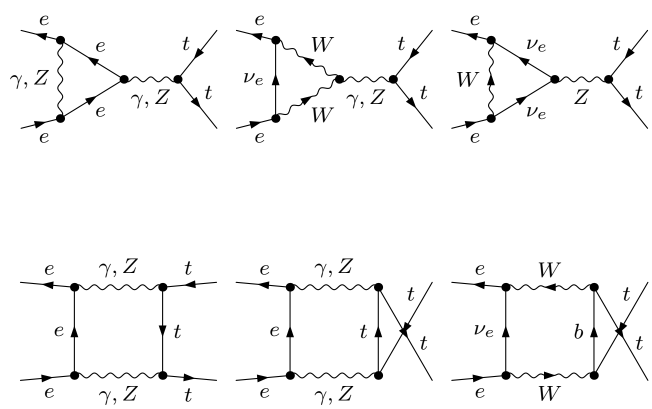

Fig. 1. Typical graphs contributing to the weak and QED corrections to $e^+e^- \to t\bar{t}$.

The virtual corrections contain both ultraviolet (UV) and infrared (IR) divergences and are treated by dimensional regularization. The UV divergences are eliminated by renormalization on the amplitude level, while the IR poles can only be eliminated at the cross-section level by including the emission of soft photons.

The real radiation contribution is evaluated using a semi-analytical integration approach with physically accessible observables as integration variables. This allows control over the numerical precision to more than four digits. The phase space with three particles in the final state is five-dimensional. However, two of the angles are trivial and may be integrated out so that

$$d\sigma = \frac{1}{(2\pi)^4}\frac{1}{2s\beta_0}|\mathcal{M}|^2\ \frac{\pi s}{16}\ drdxd\cos\theta, \tag{3}$$

where θ is the angle between the anti-top quark and the positron, $x = 2p_\gamma \cdot p_{\bar{t}}/s$ and $r = (p_t + p_{\bar{t}})^2/s$. Cuts on the energies of the photon or top quarks, or cuts on the angles between particles directly transfer into cuts on these variables. The phase space is illustrated in Fig. 2. The t ($\bar{t}$) are at rest at points A (B). Soft photons are located at point C. All phase space points away from $(r,x) = (1,0)$ are finite and can be obtained numerically for any set of reasonable cuts. The soft photon contribution is analytically removed and combined with the virtual graphs.

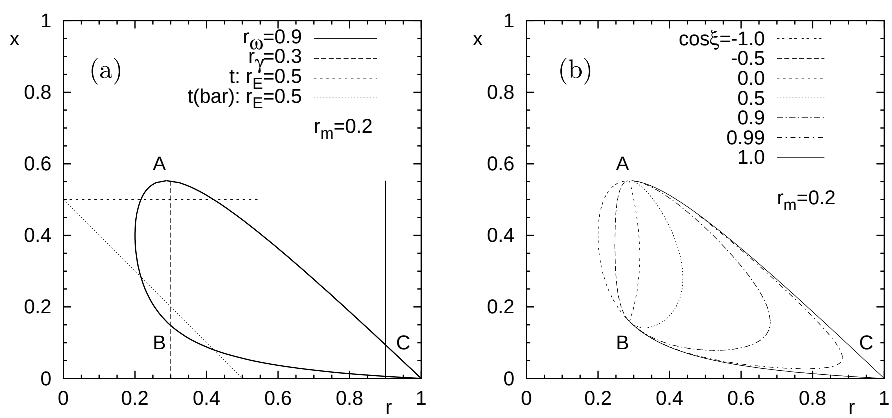

Fig. 2. Phase space for $r_m = \frac{4m_t^2}{s} = 0.2$ (non-zero top mass). Energetic cuts are also shown in (a) $r_E = 2E_t^{\min}/\sqrt{s}$, $r_{\bar{E}} = 2\bar{E}_t^{\min}/\sqrt{s}$, $r_\omega = 1-2\omega/\sqrt{s} = 1-2E_{\min}(\gamma)/\sqrt{s}$, $r_\gamma = 1 - 2E_{\max}(\gamma)\sqrt{s}$ while (b) shows different values of the acollinearity angle $\xi = \pi - \theta_{t\bar{t}}$. Note that $\cos\xi = 1$ corresponds to the elastic case.

Numerical results from `topfit` have been compared with two other groups. First the virtual and soft photon contribution have been compared with results from the Karlsruhe group [8,9]. The weak virtual corrections to the angular distributions agree to twelve digits, while the pure photonic corrections agree to at least eleven digits. Second, the hard photon corrections have been compared with results from the GRACE group [11]. Depending on the observable, agreement to three digits is generally obtained.

Fig. 3 shows the (a) total cross section and (b) forward–backward asymmetry as a function of $\sqrt{s}$.[1] The values of the input parameters can be found in Ref. [5]. The effects of radiative corrections are more dramatic for top-pairs produced close to the direction of the beam. For the ILC range of centre-of-mass energies, backward scattered top quarks give rise to slightly larger corrections to the toral cross section than forward scattered ones [8]. For higher energies this effect is more or less washed out. This is not the case for the forward–backward asymmetry.

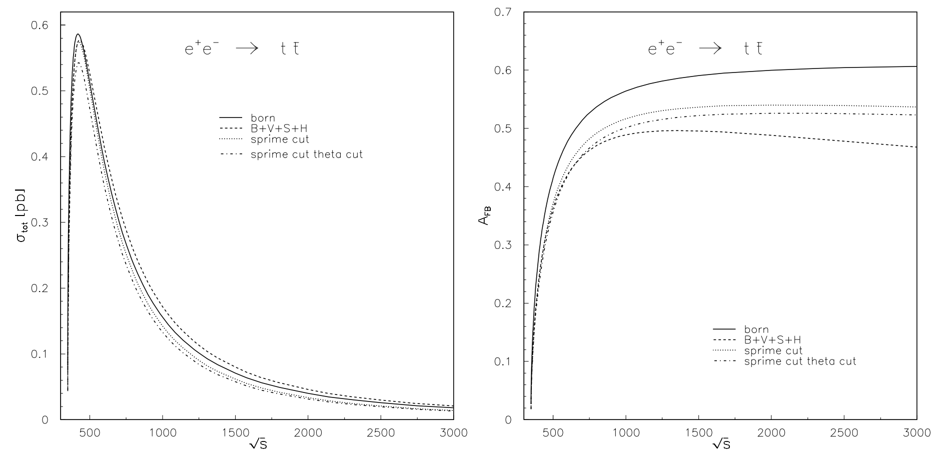

Fig. 3. The (a) total cross-section and (b) forward–backward asymmetry for top-pair production as a function of s. Born (solid lines), electroweak (dashed lines), electroweak with $s' = 0.7\,s$-cut (dotted lines) and electroweak with $s' = 0.7\,s$-cut and $\cos\theta = 0.95$-cut (dash-dotted lines).

In summary Ref. [5] shows that at the ILC, EW radiative corrections modify the differential (as well as the integrated) top-quark observables by more than the anticipated experimental precision of a few per mille. The package `topfit` provides the means to calculate those corrections and allows predictions for various realistic cuts on the scattering angle as well as on the energy of the photon. The successful comparison with Refs. [7,8] means that the technical precision of `topfit` is completely tested.

3. Polarised top quark decay [16]

In e^+e^- collisions, top quarks are produced highly polarized, especially if one tunes the polarization of the incoming beams, as possible *e.g.* at the ILC collider [2]. At the LHC the polarization of top quarks is tiny due to

[1] Note that this is a fixed-order α calculation, *i.e.* no higher order corrections such as photon exponentiation have been taken into account.

parity and time reversal invariance of QCD. However, the spins of t and $\bar{t}$ are in general highly correlated.

The polarization of the top quark is transferred to the angular distribution of its decay products through its weak, parity violating decays. If we consider a polarized ensemble of top quarks at rest with polarization vector $\boldsymbol{P}$, $0 \leq |\boldsymbol{P}| \leq 1$, the differential decay distribution with respect to the angle ϑ between $\boldsymbol{P}$ and the direction $\hat{\boldsymbol{p}}$ of a given decay product is given by,

$$\frac{1}{\Gamma}\frac{d\Gamma}{d\cos\vartheta} = \frac{1}{2}\left(1 + |\boldsymbol{P}|\kappa_p \cos\vartheta\right). \tag{4}$$

In Eq. (4), Γ is the partial width for the corresponding decay of unpolarized top quarks, and κ_p is the so-called *spin analysing power* of the final state particle or jet under consideration. For example, in the semileptonic decay $t \to l^+\nu_l b$, the charged lepton (b-quark) has spin analysing power $\kappa_p = +1$ (~ -0.41) at the tree level within the Standard Model. In hadronic top decays $t \to b\bar{d}u$ (where $d(u)$ stands generically for d, s (u, c)), the rôle of the charged lepton is played by the $\bar{d}$ quark. However, the $\bar{d}$ quark cannot be easily identified, but with a 61% probability is contained in the least energetic light (*i.e.* non-b-quark) jet. The spin analysing for the least energetic jet is denoted by κ_j.

The QCD corrections to κ_p for hadronic top decays are computed in Ref. [16]. These corrections are one ingredient in a full analysis of top quark (pair) production and decay at next-to-leading order in α_s, both at lepton and hadron colliders. They form part of the *factorizable* corrections within the pole approximation for the top quark propagator. The QCD corrections for semileptonic polarized top quark decays have been computed in Ref. [17].

TABLE I

QCD-corrected results for spin analysing powers.

	partons	jets, E-alg.	jets, D-alg.
$\kappa_{\bar{d}}$	0.9664(7)	0.9379(8)	0.9327(8)
$\delta_{\bar{d}}^{\rm QCD}$ [%]	-3.36 ± 0.07	-6.21 ± 0.08	-6.73 ± 0.08
κ_b	$-0.3925(6)$	$-0.3907(6)$	$-0.3910(6)$
$\delta_b^{\rm QCD}$ [%]	-3.80 ± 0.15	-4.24 ± 0.15	-4.18 ± 0.15
κ_u	$-0.3167(6)$	$-0.3032(6)$	$-0.3054(6)$
$\delta_u^{\rm QCD}$ [%]	$+1.39 \pm 0.19$	-2.93 ± 0.19	-2.22 ± 0.19
κ_j	—	0.4736(7)	0.4734(7)
$\delta_j^{\rm QCD}$ [%]	—	-7.18 ± 0.13	-7.21 ± 0.13

The size of the next-to-leading order (NLO) correction is defined as

$$\kappa_p \equiv \kappa_p^0[1+\delta_p^{\rm QCD}] + O(\alpha_{\rm s}^2), \tag{5}$$

where κ_p^0 denotes the Born result. Table I shows that the top-spin analysing powers of the final states in non-leptonic top quark decays receive QCD corrections in the range $+1.4\%$ to -7.2%. The spin analysing power of jets is smaller than that of the corresponding bare quarks. This has to be contrasted with the spin analysing power of the charged lepton in decays $t(\uparrow) \to bl^+\nu_l$ where the QCD corrected result (for $m_b = 0$) reads [17] $\kappa_l = 1 - 0.015\alpha_{\rm s}$, *i.e.* the correction is at the per mille level.

4. Six fermion production [18]

Since top quarks decay via the cascade $t \to bW^+ \to bf\bar{f}'$ into three fermions, the production of $t\bar{t}$ pairs corresponds to a particular class of $e^+e^- \to 6f$ processes: $e^+e^- \to b\bar{b}f_1\bar{f}_1'f_2\bar{f}_2'$, where $f_i\bar{f}_i'$ denote two weak isospin doublets as shown in Fig. 4. Ref. [18] presents the Monte Carlo event generator `Lusifer`, which is designed for all SM processes $e^+e^- \to 6$ fermions in lowest order[2]. Gluon-exchange diagrams can be included for final states with two leptons and four quarks (not yet for six-quark final states). The matrix elements are evaluated using the Weyl–van der Waerden (WvdW) spinor technique and the phase-space integration is performed using multi-channel Monte Carlo integration improved by adaptive weight optimization. The lowest-order predictions are dressed by initial-state radiation (ISR) in the leading logarithmic approximation following the structure-function approach [22].

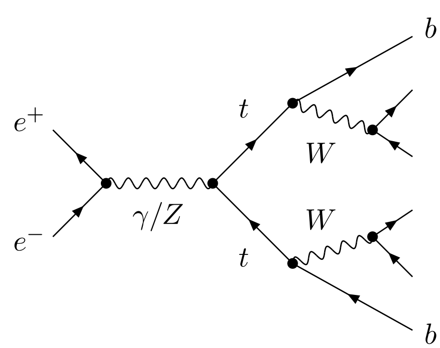

Fig. 4. Diagram for $t\bar{t}$ production: $e^+e^- \to t\bar{t} \to bW^+\bar{b}W^- \to 6f$.

[2] Note that Ref. [19] describes similar results based on the HELAC/PHEGAS [20] and AMEGIC++ [21] packages.

There is a technical problem due to the finite decay widths of unstable particles in the amplitudes which generates gauge-invariance-breaking effects. Already for CM energies in the TeV range these effects are clearly visible in some cases, underlining the importance of this issue. Within `Lusifer` several width schemes are implemented, including the *complex-mass scheme*, which was introduced in Ref. [23] for tree-level predictions and maintains gauge invariance. Hence, gauge-violating artefacts can be controlled by comparing a given width scheme with the complex-mass scheme.

Figure 5(a) illustrates the energy dependence of the top-quark pair production cross section for final states where one of the produced W bosons decays hadronically and the other leptonically. The cross section steeply rises

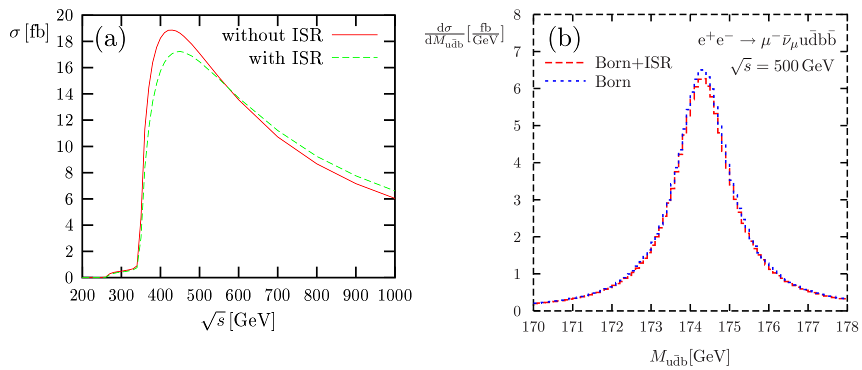

Fig. 5. (a) Total cross section of $e^+e^- \to \mu^-\bar{\nu}_\mu u\bar{d}b\bar{b}$ (without gluon-exchange diagrams) as function of the CM energy with and without ISR and (b) Invariant-mass distribution of the $u\bar{d}b$ quark triplet in $e^+e^- \to \mu^-\bar{\nu}_\mu u\bar{d}b\bar{b}$ (without gluon-exchange diagrams): absolute prediction with and without ISR.

at the $t\bar{t}$ threshold, reaches its maximum between 400 GeV and 500 GeV, and then decreases with increasing energy. We see that ISR reduces the cross section for energies below its maximum and enhances it above, thereby shifting the maximum to a higher energy. This behaviour is simply due to the radiative energy loss induced by ISR. Near a CM energy of 250 GeV the onset of WWZ production can be observed. Note that this contribution is entirely furnished by background diagrams, *i.e.* by diagrams that do not have a resonant top-quark pair. Figure 5(b) shows the invariant-mass distribution of the $u\bar{d}b$ quark triplet that results from the top-quark decay. As expected, ISR does not distort the resonance shape but merely rescales the Breit–Wigner-like distribution.

Table II shows the effect of using different schemes for introducing finite decay widths. In spite of violating gauge invariance, the fixed width practically yields the same results as the complex-mass scheme that maintains gauge invariance. Table II also shows some results obtained from the multipurpose packages `Whizard` [24] and `Madgraph` [25]. In general, and apart from a few cases, where the limitations of `Whizard` and `Madgraph` become visible, there is good numerical agreement, demonstrating the reliability of `Lusifer`.

TABLE II

Born cross sections (without ISR and gluon-exchange diagrams) for $e^+e^- \to \mu^-\bar{\nu}_\mu u\bar{d}b\bar{b}$ for various CM energies and schemes for introducing decay widths.

$\sigma(e^+e^- \to \mu^-\bar{\nu}_\mu u\bar{d}b\bar{b})$ [fb]				
$\sqrt{s}$[GeV]		500	800	2000
`Lusifer`	fixed width / step width	17.095(11)	8.6795(83)	1.8631(31)
	running width	17.106(10)	8.6988(85)	2.3858(31)
	complex mass	17.085(10)	8.6773(84)	1.8627(31)
`W.&M.`	step width	17.1025(80)	8.6823(44)	1.8657(12)

5. Top production in the asymptotic regime [15, 26–29]

At energies far above the electroweak scale, $\sqrt{s} \gg M \sim M_W \sim M_Z$, the electroweak corrections are enhanced by large logarithmic corrections of the type

$$\alpha^L \log^N\left(\frac{s}{M^2}\right), \qquad 1 \le N \le 2L.$$

The leading logarithmic corrections correspond to $N = 2L$. These corrections are related to the singular part of the radiative corrections in the massless limit $M^2/s \to 0$. They are either remnants of UV singularities or mass singularities from soft/collinear emission of virtual or real particles from initial or final state particles. This is because the mass of the gauge bosons provide a physical cut-off to the real radiation. Furthermore, the Bloch–Nordsieck theorem is violated for inclusive quantities if the asympototic states carry non-Abelian charges.

The top quark effective vertex of Eq. (2) receives logarithmic corrections in the asymptotic limit. In fact, it is possible to see immediately from the structure of the one-loop Feynman diagrams of both the SM and the MSSM that the coefficients of the new extra Lorentz structure $(p-p')^\mu$ vanish at large q^2 like $1/q^2$, while those of the conventional Lorentz structures (γ^μ, $\gamma^\mu\gamma^5$) can produce either quadratic or linear logarithms. Therefore, the leading terms of $t\bar{t}$ production at asymptotic energies are exactly those that would be computed in a conventional scheme in which the new scalar component of Eq.(2) has been neglected, and four independent gauge-invariant combinations survive that are, formally, equivalent to those of the final light quark case.

Within the SM, typical diagrams giving rise to these logarithms are shown in Fig. 6. The one-loop logarithmic corrections in the SM have been

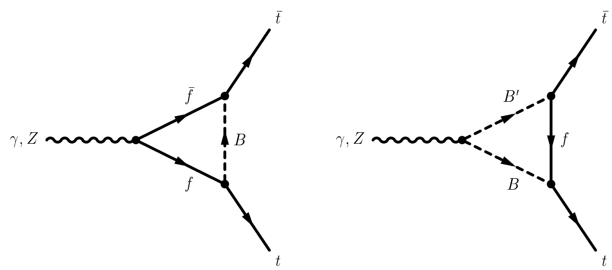

Fig. 6. Triangle SM diagrams contributing to the asymptotic logarithmic behaviour in the energy; f represent t or b quarks, B represent $W^{\pm}$, $\Phi^{\pm}$ or Z, G^0, $H_{\rm SM}$.

computed in Ref. [15] for the integrated $e^+e^- \to t\bar{t}$ cross section, σ_t,

$$\sigma_t = \sigma_t^B\left(1+\frac{\alpha}{4\pi}\left((8.87N-33.16)\ln\frac{q^2}{\mu^2}+\left(22.79\ln\frac{q^2}{M_W^2}-5.53\ln^2\frac{q^2}{M_W^2}\right)\right.\right.$$
$$\left.\left.+\left(3.52\ln\frac{q^2}{M_Z^2}-1.67\ln^2\frac{q^2}{M_Z^2}\right)-14.21\ln\frac{q^2}{m_t^2}\right)\right), \qquad (6)$$

the forward backward asymmetry $A_{{\rm FB},t}$,

$$A_{{\rm FB},t} = A_{{\rm FB},t}^B+\frac{\alpha}{4\pi}\left((0.45N-4.85)\ln\frac{q^2}{\mu^2}-\left(1.79\ln\frac{q^2}{M_W^2}+0.17\ln^2\frac{q^2}{M_W^2}\right)\right.$$
$$\left.-\left(1.26\ln\frac{q^2}{M_Z^2}+0.06\ln^2\frac{q^2}{M_Z^2}\right)+0.61\ln\frac{q^2}{m_t^2}\right), \qquad (7)$$

the longitudinal polarization asymmetry $A_{{\rm LR},t}$ and its forward–backward polarization asymmetry A_t. The MSSM effects have also been computed [15]. The effects are largest for the total cross section as shown in Fig. 7.

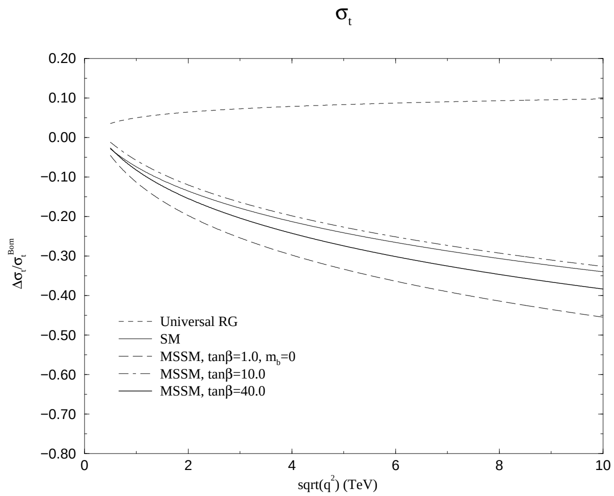

Fig. 7. Relative effects on the $t\bar{t}$ cross section $\Delta\sigma_t/\sigma_t$ in e^+e^- annihilation at CM energy $\sqrt{q^2}$ due to the asymptotic logarithmic terms.

The conclusion is that the leading electroweak effect at the one-loop level is quite sizeable in the TeV region in all observables, with the only (expected) exception of the forward–backward asymmetry. These effects are systematically larger than those in the corresponding lepton or "light" (u, d, s, c, b) quark production observables, both in the SM and MSSM. In the latter case, top production exhibits also in the leading terms a strong dependence on $\tan\beta$, much stronger than that of bottom production.

In the asymptotic region, the different effects on the $t\bar{t}$ and $b\bar{b}$ cross sections can in principle be exploited [26–29]. Refs. [29] examine the effect at the LHC under the assumption of a "moderately" light SUSY scenario and find that the electroweak and the strong SUSY contributions combine to produce an enhanced effect whose relative value in the $t\bar{t}$ and $b\bar{b}$ cross sections could be as large as 20% for large values of $\tan\beta$.

6. Top quark couplings

6.1. Wtb [30]

The most general CP-conserving Wtb vertex can be parameterised with the effective Lagrangian given by[3]

[3] The most general Wtb vertex (up to dimension five) involves ten operators, but at the expected level of precision it is an excellent approximation to consider the top on-shell. With b also on-shell and $W \to l\nu, jj$ six of them can be eliminated using Gordon identities. The resulting Lagrangian can be further restricted assuming CP conservation. The couplings can then be taken to be real, of either sign.

$$\mathcal{L} = -\frac{g}{\sqrt{2}}\bar{b}\,\gamma^\mu \left(V_{tb}^L P_\mathrm{L} + V_{tb}^R P_\mathrm{R}\right) t\, W_\mu^- \\ -\frac{g}{\sqrt{2}}\bar{b}\,\frac{i\sigma^{\mu\nu}q_\nu}{M_W}\left(g^L P_\mathrm{L} + g^R P_\mathrm{R}\right) t\, W_\mu^- + \mathrm{h.c.} \tag{8}$$

In the SM the Wtb vertex is purely left-handed and its size is given by the Cabibbo–Kobayashi–Maskawa (CKM) matrix element $V_{tb}^L \equiv V_{tb}$. The right-handed vector and both tensor couplings vanish at tree-level in the SM, but can be generated at higher orders in the SM or its extensions [1]. Note that V_{tb}^R is constrained by $b \to s\gamma$ decays while the $\sigma^{\mu\nu}$ terms are not because of the extra q^μ factor that suppresses their effect in b decays. The Wtb vertex structure can be probed and measured using either top-pair production or single-top-quark production processes. The $t\bar{t}$ cross-section is rather insensitive to the size of V_{tb} and to obtain a measure of the *absolute* value of V_{tb} it is necessary to fall back on less abundant single top production [31], with a rate proportional to $|V_{tb}|^2$. Nevertheless, $t\bar{t}$ production can give invaluable information on the Wtb vertex. Angular asymmetries between decay products are very sensitive to a small admixture of a right-handed γ^μ term or a $\sigma^{\mu\nu}$ coupling of either chirality.

In Ref. [30], the forward–backward asymmetry in the decay of the top quark $t \to W^+ b \to l^+\nu b$ as measured in the W rest frame is proposed as a particularly sensitive probe of anomalous top quark couplings. It is defined as

$$A_\mathrm{FB} = \frac{N(x_{bl} > 0) - N(x_{bl} < 0)}{N(x_{bl} > 0) + N(x_{bl} < 0)}\,, \tag{9}$$

where x_{bl} is the cosine of the angle between the 3-momenta of the b quark and the charged lepton in the W rest frame, and N stands for the number of events. The same definition holds for the $\bar{t} \to l^-\bar{\nu}\bar{b}$ decay.

A_FB only depends on the t, b and W boson masses, and on the couplings in Eq. (8). The SM tree-level (LO) value is $A_\mathrm{FB} = 0.2223$ while the bulk effect of the one-loop QCD corrections can be taken into account by including a $\sigma^{\mu\nu}$ term $g^R = -0.00642$ [32]. The corresponding NLO value is $A_\mathrm{FB} = 0.2257$. In Fig. 8 we plot A_FB for different values of $\delta g^R \equiv g^R + 0.00642$, $\delta g^L \equiv g^L$ and $\delta V_{tb}^R \equiv V_{tb}^R$. Numerical studies of the tree-level $2 \to 6$ processes gg, $q\bar{q} \to t\bar{t} \to W^+ b W^- \bar{b} \to l\nu jjjj$ plus $Wjjjj$ background, including all spin correlations and realistic cuts suggest that a statistical error of $\delta A_\mathrm{FB} \simeq 5 \times 10^{-4}$ is achievable at the LHC. The main systematic errors come from the uncertainty in m_t and M_W and will be negligible with ILC precision.

The cross sections in the forward and backward hemispheres are of the order of 11–16 pb (2–3 pb) for the signal (background). Using both electron

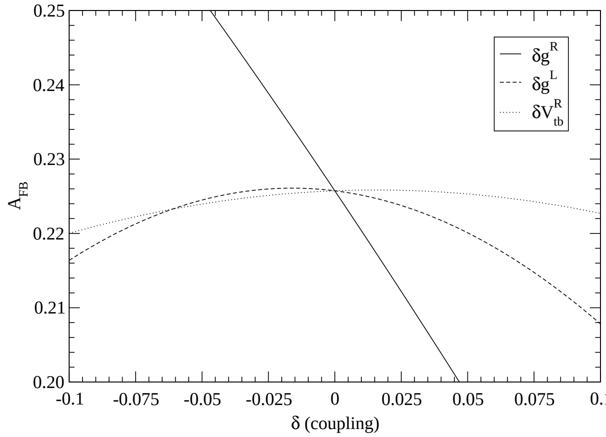

Fig. 8. Dependence of $A_{\rm FB}$ on δg^R (solid line), δg^L (dashed line) and δV_{tb}^R (dotted line). The SM result occurs where all three lines cross. We use $m_t = 175$, $M_W = 80.33$, $m_b = 4.8$ GeV.

and muon channels leads to a (statistical) sensitivity of $\delta g^R = \pm 0.003$, $\delta g^L = +0.02(-0.05)$ and $\delta V_{tb}^R = +0.08(-0.04)$. The sensitivity to g^R is one order of magnitude better than in single top production at LHC [33] while the sensitivity to g^L is competitive with that expected at the ILC, or from single top production at LHC.

6.2. Flavour Changing Neutral Couplings [34–37]

Flavor Changing Neutral (FCN) decays of the top quark within the strict context of the Standard Model are known to be extremely rare. In fact, there are no tree-level FCN current processes in the Standard Model. However, they can be generated at the one-loop level by charged current interactions. The most general effective Lagrangian describing the possible interactions of a top quark, a light quark q and a Z boson, photon A, gluon G or Higgs H can be written as,

$$\begin{aligned} \mathcal{L} \;=\; & -\frac{g'}{2}\, X_{tq}\, \bar{t}\gamma_\mu (x^L_{tq} P_{\rm L} - x^R_{tq} P_{\rm R}) q Z^\mu - \frac{g'}{2}\, \kappa_{tq}\, \bar{t}(\kappa^v_{tq} + \kappa^a_{tq}\gamma_5)\frac{i\sigma_{\mu\nu}q^\nu}{m_t} q Z^\mu \\ & -e\, \lambda_{tq}\, \bar{t}(\lambda^v_{tq} + \lambda^a_{tq}\gamma_5)\frac{i\sigma_{\mu\nu}q^\nu}{m_t} q A^\mu - g_s \zeta_{tq} \bar{t}\left(\zeta^V_{tq} + \zeta^A_{tq}\gamma_5\right)\frac{i\sigma_{\mu\nu}q^\nu}{m_t} q T^a G^{a\mu} \\ & -\frac{g}{2\sqrt{2}} g_{tg} \bar{t}\left(g^V_{tq} + g^Q_{tq}\gamma_5\right) qH + .\text{h.c.}\,, \end{aligned} \tag{10}$$

where $g' = g/\cos\theta_W$, $P_{\rm R,L} = (1 \pm \gamma_5)/2$. The chirality-dependent couplings are constants and are normalized to $(x^L_{tq})^2 + (x^R_{tq})^2 = 1$ *etc.* Within the

SM, all of these vertices vanish at the tree-level, but can be generated at one-loop by charged current interactions. However, because of GIM cancellations, the one-loop effects are parametrically suppressed beyond naive expectations based on pure dimensional analysis, power counting and CKM matrix elements by m_b^4/M_W^4. The Standard Model typical branching ratios for these rare top quark decays are so small ($\sim 10^{-12}$–10^{-17}) that they are hopelessly undetectable at the Tevatron, LHC and ILC in any of their scheduled upgradings.

Refs. [34, 35] considered loop induced $t \to ch$ and $t \to cg$ FCN decays in the MSSM and in the general two-Higgs doublet model (2HDM) — see also Ref. [39, 40]. Typical diagrams contributing to these decays are shown in Fig. 9. The 2HDM parameter space is constrained by the ρ parameter and the one-loop corrections to the ρ-parameter from the 2HDM sector cannot deviate from the reference SM contribution by more than one per mille, $|\delta\rho^{\rm 2HDM}| < 0.001$. There are also constraints on the charged Higgs from radiative B decays. Nevertheless the fiducial branching ratio defined by

$$B^j(t \to X + c) = \frac{\Gamma^j(t \to X + c)}{\Gamma(t \to W^+ + b) + \Gamma^j(t \to H^+ + b)} \,, \qquad (11)$$

may be as large as 10^{-5} for top decay into the lightest CP-even Higgs and 10^{-6} for $t \to gc$. Values for other models are reviewed in [37].[4]

To illustrate the potential effects in a 2HDM model, Fig. 10 shows the branching ratios for $t \to Xc$ for $X = h, H,\ g$ as functions of the parameters α and β. The highest potential rates are of order 10^{-5}, and so there is hope for being visible.

Current limits on FCN top decays from the Tevatron, LEP and HERA are at the few per cent level. Run 2 at the Tevatron is expected to reduce these limits by about an order of magnitude. At the LHC, the search for FCN top couplings can be carried out examining two different types of processes. On the one hand, we can look for FCN top decays in $gg, q\bar{q} \to t\bar{t} \to XqWb$ where $X = \gamma, Z, g$ or Higgs. On the other hand, one can search for single top production via an anomalous effective vertex such as $qg \to Xt$ where the top quark is assumed to decay in the SM dominant mode $t \to Wb$ — see for example Ref. [41]. The main backgrounds are thus $t\bar{t}$, $W +$ jets, $VV +$ jets and single top production. Numerical simulations of signal and background indicate that the LHC will improve by at least a factor of 10 on the Tevatron sensitivity to around 10^{-5}.

At the ILC, the top pair production cross section is much smaller than at the LHC and the limits obtained from top decays cannot compete with those

[4] Note that the related decay $H \to t\bar{c}$ is discussed in the context of the 2HDM in [38]. The isolated top quark signature, unbalanced by any other heavy particle should help to identify the FCN event and makes branching ratios of 10^{-5} accessible at the LHC.

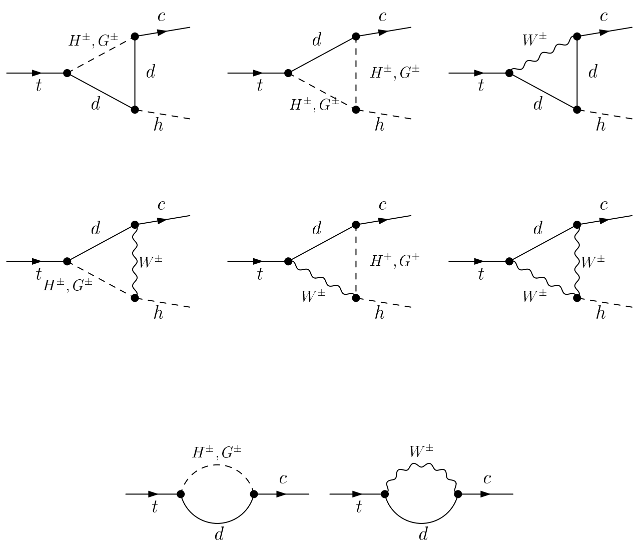

Fig. 9. One-loop vertex diagrams contributing to the FCN top quark decays. Shown are the vertices and mixed self-energies with all possible contributions from the SM fields and the Higgs bosons from the general 2HDM.

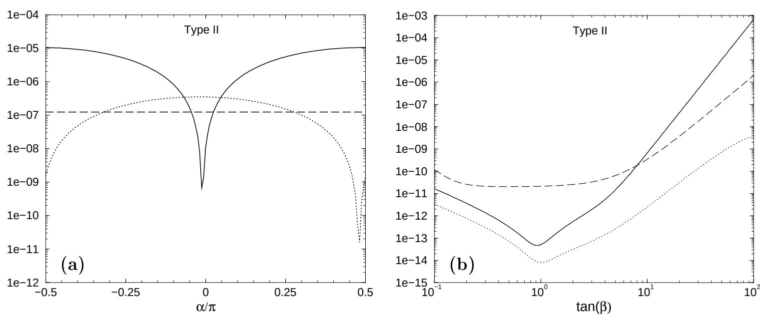

Fig. 10. Evolution of the FCNC top quark fiducial ratios in Type II 2HDM as functions of (a) the mixing angle α in the CP-even Higgs sector, and (b) $\tan\beta$ for $t \to Xc$ with $X = h$ (solid), $X - H$ (dotted) and $X = g$ (dash). The plot in (b) continues above the usual bound on $\tan\beta$ just to better show the general trend.

from the LHC. The capabilities of the ILC have been studied in Ref. [36] for the single top production processes $e^+e^- \to tq$ shown in Fig. 11 and $e^+e^- \to tq\gamma$ and $e^+e^- \to tqZ$. The signal matrix elements including the top decay were evaluated using HELAS [44] and introducing a new HELAS-like subroutine `IOV2XX` to compute the non-renormalizable $\sigma_{\mu\nu}$ vertex. The relevant backgrounds are $e^+e^- \to W^+q\bar{q}'$, $W^+q\bar{q}'Z$ and $W^+q\bar{q}'\gamma$ and were evaluated using MadGraph [25].

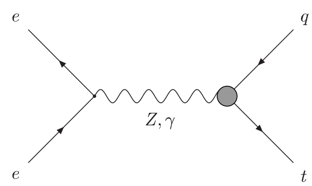

Fig. 11. Feynman diagrams for $e^+e^- \to t\bar{q}$ via Ztq or γtq FCN couplings. The top quark is off-shell and decays to Wb.

Assuming one year of running time in all the cases, that is, 100 fb^{-1} for LHC, 300 fb^{-1} for ILC at 500 GeV and no beam polarisation, Refs. [36, 42] find that by combining the information from both production and decay, the sensitivities on the $t \to Xc$ coupling are given in Table III. The most optimistic case with 500 fb^{-1} of data 80% polarised electron and 60% polarised positron beams and a CM energy of 800 GeV is denoted by ILC+.

TABLE III

3σ discovery limits on top FCN couplings that can be obtained at LHC and ILC for one year of operation.

	LHC	ILC	ILC+
$\mathrm{Br}(t \to Zc)$ (γ_μ)	3.6×10^{-5}	1.9×10^{-4}	1.9×10^{-4}
$\mathrm{Br}(t \to Zc)$ $(\sigma_{\mu\nu})$	3.6×10^{-5}	1.8×10^{-5}	7.2×10^{-6}
$\mathrm{Br}(t \to \gamma c)$	1.2×10^{-5}	1.0×10^{-5}	3.8×10^{-6}

We see that LHC and ILC complement each other in the search for top FCN vertices. The γ_μ couplings to the Z boson can be best measured or bound at LHC, whereas the sensitivity to the $\sigma_{\mu\nu}$ ones is better at ILC. For a more detailed discussion, see Ref. [37].

7. Impact of a precise top mass measurement [45, 46]

The current world average for the top-quark mass is $m_t = 178.0 \pm 4.3$ GeV [47, 48]. The expected accuracy at the Tevatron and the LHC is $\delta m_t =$ 1–2 GeV [1], while at the ILC a very precise determination of m_t with an accuracy of $\delta m_t \lesssim 100$ MeV should be possible [2–4, 49]. This error contains both the experimental error of the mass parameter extracted from the $t\bar{t}$ threshold measurements at the ILC and the expected theoretical uncertainty from its transition into a suitable short-distance mass (like the $\overline{\mathrm{MS}}$ mass).

7.1. Electroweak Precision Observables

Electroweak Precision Observables (EWPO) can be used to perform internal consistency checks of the model under consideration and to obtain indirect constraints on unknown model parameters. This is done by comparing experimental results for the precision observables with their theory prediction within, for example, the Standard Model (SM). Any improvement in the precision of the measurement of m_t will have an effect on the analysis of EWPO of which the two most prominent are the W boson mass M_W and the effective leptonic mixing angle $\sin^2\theta_{\rm eff}$.

Currently the uncertainty in m_t is by far the dominant effect in the theoretical uncertainties of the EWPO. Today's experimental errors of M_W and $\sin^2\theta_{\rm eff}$ [50] are shown in Table IV, together with the prospective future experimental errors at high energy colliders (see [51] for a compilation of these errors and additional references).

TABLE IV

Experimental errors of M_W and $\sin^2\theta_{\rm eff}$ at present and future colliders [50, 51].

	Today	Tevatron/LHC	ILC	GigaZ
$\delta\sin^2\theta_{\rm eff}(\times 10^5)$	16	14–20	—	1.3
δM_W [MeV]	34	15	10	7

In general, there are two sources of theoretical uncertainties: those from unknown higher-order corrections ("intrinsic" theoretical uncertainties), and those from experimental errors of the input parameters ("parametric" theoretical uncertainties). The intrinsic uncertainties within the SM are

$$\Delta M_W^{\rm intr,today} \approx 4~{\rm MeV}, \qquad \Delta\sin^2\theta_{\rm eff}^{\rm intr,today} \approx 4.9\times 10^{-5} \tag{12}$$

at present [52, 53]. They are based on the present status of the theoretical predictions in the SM, namely the complete two-loop result for M_W (see [52, 54] and references therein), the complete two-loop fermionic result for $\sin^2\theta_{\rm eff}$ (see [53], previous partial results and references can be found in [55]) and leading three-loop contributions to both observables (see [56] for the latest result, and references therein).

The current parametric uncertainties induced by the experimental errors of m_t [57] are

$$\delta m_t = 4.3~{\rm GeV} \Rightarrow \Delta M_W^{{\rm para},m_t} \approx \pm 26~{\rm MeV}, \quad \Delta\sin^2\theta_{\rm eff}^{{\rm para},m_t} \approx \pm 14\times 10^{-5}. \tag{13}$$

We see that the parametric uncertainties of M_W and $\sin^2\theta_{\rm eff}$ induced by δm_t are approximately as large as the current experimental errors.[5]

A future experimental error of $\delta m_t \approx 1.5$ GeV at the LHC will give rise to parametric uncertainties of

$$\Delta M_W^{\rm para,LHC} \approx 9 \text{ MeV}, \qquad \Delta\sin^2\theta_{\rm eff}^{\rm para,LHC} \approx 4.5\times 10^{-5}.$$

On the other hand, the ILC precision of $\delta m_t \approx 0.1$ GeV will reduce the parametric uncertainties to

$$\Delta M_W^{\rm para,ILC} \approx 1 \text{ MeV}, \qquad \Delta\sin^2\theta_{\rm eff}^{\rm para,ILC} \approx 0.3\times 10^{-5}.$$

In order to keep the theoretical uncertainty induced by m_t at a level comparable to or smaller than the other parametric and intrinsic uncertainties, δm_t has to be smaller than about 0.2 GeV in the case of M_W, and about 0.5 GeV in the case of $\sin^2\theta_{\rm eff}$. In other words, ILC accuracy on m_t will be necessary in order to keep the parametric error induced by m_t at or below the level of the other uncertainties. With the LHC accuracy on m_t, on the other hand, δm_t will be the dominant source of uncertainty.

As an example of the potential of a precise measurement of the EWPO to explore the effects of new physics, Fig. 12 shows the predictions for M_W and $\sin^2\theta_{\rm eff}$ in the SM in comparison with the prospective experimental accuracy obtainable at the LHC and the ILC without GigaZ option (labelled as LHC/ILC) and with the accuracy obtainable at an ILC with GigaZ option (labelled as GigaZ). The current experimental values are taken as the central ones [50]. For the Higgs boson mass a future measured value of $m_h = 115$ GeV has been assumed (in accordance with the final lower bound obtained at LEP [58]). We see that the improvement in δm_t from $\delta m_t = 2$ GeV to $\delta m_t = 0.1$ GeV strongly reduces the parametric uncertainty in the prediction for the EWPO and leads to a reduction by about a factor of 10 in the allowed parameter space of the M_W–$\sin^2\theta_{\rm eff}$ plane.

7.2. Indirect determination of the SM top Yukawa coupling

A high precision on m_t is also important to obtain indirect constraints on the top Yukawa coupling y_t from EWPO [59]. The top Yukawa coupling enters the SM prediction of EWPO starting at $\mathcal{O}(\alpha\alpha_t)$ [60]. Indirect bounds on this coupling can be obtained if one assumes that the usual relation between the Yukawa coupling and the top quark mass, $y_t = \sqrt{2}m_t/v$ (where v is the vacuum expectation value), is modified.

[5] Note that the parametric errors induced by $\delta(\Delta\alpha_{\rm had})$ are $\Delta M_W^{{\rm para},\Delta\alpha_{\rm had}} \approx \pm 6.5$ MeV and $\Delta\sin^2\theta_{\rm eff}^{{\rm para},\Delta\alpha_{\rm had}} \approx \pm 13\times 10^{-5}$ [57].

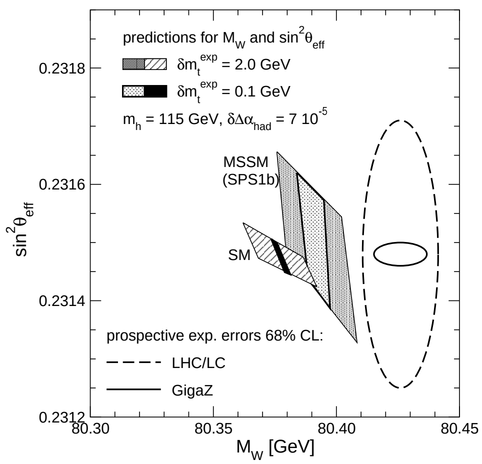

Fig. 12. The predictions for M_W and $\sin^2\theta_{\rm eff}$ in the SM and MSSM. The inner area corresponds to $\delta m_t^{\rm exp} = 0.1$ GeV (ILC), while the outer area arises from $\delta m_t^{\rm exp} = 2$ GeV (LHC). The anticipated experimental errors on M_W and $\sin^2\theta_{\rm eff}$ at the LHC/ILC and at an ILC with GigaZ option are indicated.

Assuming a precision of $\delta m_t = 2$ GeV, an indirect determination of y_t with an accuracy of only about 80% can be obtained from the EWPO measured at an LC with GigaZ option. A precision of $\delta m_t = 0.1$ GeV, on the other hand, leads to an accuracy of the indirect determination of y_t of about 40% which is competitive with the indirect constraints from the $t\bar{t}$ threshold [61]. These indirect determinations of y_t represent an independent and complementary approach to the direct measurement of y_t via $t\bar{t}H$ production at the ILC, which of course provides the highest accuracy [2].

7.3. The MSSM

Within the MSSM, EWPO are also heavily influenced by the accuracy of the top quark mass. However, the available results beyond one-loop order are less advanced than in the SM (for the latest two-loop results, see [59] and references therein). Thus, the intrinsic uncertainties in the MSSM are still considerably larger than the ones quoted for the SM in Eq. (12). Fig. 12 also shows the predictions for M_W and $\sin^2\theta_{\rm eff}$ in the MSSM where the MSSM parameters have been chosen in this example according to the reference point SPS 1b [62], and all SUSY parameters have been varied within realistic error intervals. In the MSSM case, where many additional parametric uncertainties enter, a reducing δm_t from 2 GeV to 0.1 GeV leads to reduction in the allowed parameter space of the M_W–$\sin^2\theta_{\rm eff}$ plane by a factor of more than 2.

Because of the additional symmetry of the MSSM, a precise knowledge of m_t yields additional constraints. For example, and in contrast to the SM, where the Higgs boson mass is a free input parameter, the mass of the lightest CP-even Higgs boson in the MSSM can be predicted in terms of other parameters of the model. Thus, precision measurements in the Higgs sector of the MSSM have the potential to play a similar role as the "conventional" EWPO for constraining the parameter space of the model and possible effects of new physics.

Fig. 13 shows the impact of the experimental error of m_t on the prediction for m_h in the MSSM. The parameters are chosen according to the $m_h^{\max}$ benchmark scenario [64]. The band in the left plot corresponds to the present experimental error of m_t [47, 48], while in the right plot the situation at the LHC ($\delta m_t = 1, 2$ GeV) is compared to the ILC ($\delta m_t = 0.1$ GeV). The figure shows that the ILC precision on m_t will be necessary in order to match the experimental precision of the m_h determination with the accuracy of the theory prediction (assuming that the intrinsic theoretical uncertainty can be reduced to the same level, see Ref. [65]).

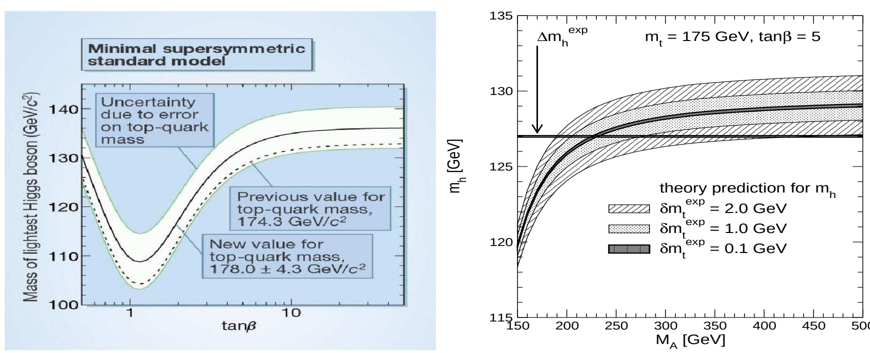

Fig. 13. Prediction for m_h in the $m_h^{\max}$ scenario of the MSSM as a function of $\tan\beta$ (left) and M_A (right). In the left plot [63] the impact of the present experimental error of m_t on the m_h prediction is shown. The three bands in the right plot [45] correspond to $\delta m_t = 1, 2$ GeV (LHC) and $\delta m_t = 0.1$ GeV (ILC). The anticipated experimental error on m_h at the ILC is also indicated.

Further examples of the importance of a precise determination of m_t in the MSSM are the prediction of sparticle masses, parameter determinations, and the reconstruction of the supersymmetric high scale theory [45].

8. Other topics

Other topics of relevance to top quark physics are discussed in the Higgs and Electroweak reviews [66, 67].

The SM Higgs boson can be searched for in the channels $p\bar{p}/pp \to t\bar{t}H + X$ at the Tevatron and the LHC. The cross sections for these processes and the final-state distributions of the Higgs boson and top quarks are presented at next-to-leading order QCD in Refs. [68, 69]. The impact of the corrections on the total cross sections is characterized by K factors, the ratio of next-to-leading order and leading order cross sections. At the central scale $\mu_0 = (2m_t + M_H)/2$, the K factors are found to be slightly below unity for the Tevatron ($K \sim 0.8$) and slightly above unity for the LHC ($K \sim 1.2$). Including the corrections significantly stabilizes the theoretical predictions for total cross sections and for the distributions in rapidity and transverse momentum of the Higgs boson and top quarks.

The two-loop corrections to the heavy quark form factor are studied in Ref. [70] where closed analytic expressions of the electromagnetic vertex form factors for heavy quarks at the two-loop level in QCD are presented for arbitrary momentum transfer. This calculation represents a first step towards the two-loop QCD corrections to $t\bar{t}$ production in both electron-positron annihilation and hadron collisions.

9. Summary and outlook

There has been significant progress in the study of top quark physics at current and future particle colliders during the past four years. As detailed above, the network has contributed to an improved knowledge of the top quark production and decay properties, both within and without the SM. However, much work remains to be carried out. In particular, although the one-loop strong and weak corrections to the top-pair production cross section are well known, the two-loop QCD corrections are needed to match the experimental accuracy. Similarly, it may be necessary to make more precise predictions of the single top cross section. Experimental studies of the observability of FCN decays of the $t \to Hc$ and $t \to gc$ decays are also needed.

Finally, we note that the treatment of unstable particles close to resonance suffers from the breakdown of ordinary perturbation theory. A toy model showing how to systematically improve the calculational accuracy order by order in perturbation theory has recently been proposed [71, 72]. We anticipate that application of this improved theoretical approach to the $t\bar{t}$ cross section close top threshold should yield an even more accurate experimental determination of the top quark mass at the ILC. Because of the large sensitivity of the Higgs boson mass to m_t, this will have an inevitable knock on in any model where the Higgs mass can be predicted from the other parameters of the theory.

REFERENCES

[1] M. Beneke *et al.*, `hep-ph/0003033`.

[2] J. Aguilar-Saavedra *et al.*, `hep-ph/0106315`.

[3] T. Abe *et al.*, `hep-ex/0106055, hep-ex/0106056, hep-ex/0106057, hep-ex/0106058`.

[4] K. Abe *et al.* `hep-ph/0109166`.

[5] J. Fleischer, A. Leike, T. Riemann, A. Werthenbach, *Eur. Phys. J.* **C31**, 37 (2003).

[6] J. Fleischer, A. Leike, T. Riemann, A. Werthenbach, `hep-ph/0211428`.

[7] J. Fleischer, J. Fujimoto, T. Ishikawa, A. Leike, T. Riemann, Y. Shimizu, A. Werthenbach, `hep-ph/0203220`.

[8] J. Fleischer, T. Hahn, W. Hollik, T. Riemann, C. Schappacher, A. Werthenbach, `hep-ph/0202109`.

[9] T. Hahn, W. Hollik, A. Lorca, T. Riemann, A. Werthenbach, `hep-ph/0307132`.

[10] J. Fujimoto, Y. Shimizu, *Mod. Phys. Lett.* **3A**, 581 (1988).

[11] F. Yuasa *et al.*, *Prog. Theor. Phys. Suppl.* **138**, 18 (2000).

[12] W. Beenakker, S. van der Marck, W. Hollik, *Nucl. Phys.* **B365**, 24 (1991).

[13] W. Hollik, C. Schappacher, *Nucl. Phys.* **B545**, 98 (1999).

[14] D. Bardin, L. Kalinovskaya, G. Nanava, `hep-ph/0012080`.

[15] M. Beccaria, F.M. Renard, C. Verzegnassi, *Phys. Rev.* **D63**, 053013 (2001).

[16] A. Brandenburg, Z.G. Si, P. Uwer, *Phys. Lett.* **B539**, 235 (2002).

[17] M. Jezabek, J.H. Kühn, *Nucl. Phys.* **B320**, 20 (1989); A. Czarnecki, M. Jezabek, J.H. Kühn, *Nucl. Phys.* **B351**, 70 (1991).

[18] S. Dittmaier, M. Roth, *Nucl. Phys.* **B642**, 307 (2002).

[19] T. Gleisberg, F. Krauss, C.G. Papadopoulos, A. Schaelicke, S. Schumann, *Eur. Phys. J.* **C34**, 173 (2004).

[20] A. Kanaki, C.G. Papadopoulos, `hep-ph/0012004`.

[21] A. Schalicke, F. Krauss, R. Kuhn, G. Soff, *J. High Energy Phys.* **0212**, 013 (2002).

[22] E.A. Kuraev, V.S. Fadin, *Yad. Fiz.* **41**, 753 (1985) [*Sov. J. Nucl. Phys.* **41**, 466 (1985)]; G. Altarelli, G. Martinelli, in *"Physics at LEP"*, eds. J. Ellis and R. Peccei, CERN 86-02 (CERN, Geneva, 1986), Vol. 1, p. 47; O. Nicrosini, L. Trentadue, *Phys. Lett.* **B196**, 551 (1987); *Z. Phys.* **C39**, 479 (1988); F.A. Berends, W.L. van Neerven, G.J. Burgers, *Nucl. Phys.* **B297**, 429 (1988); Erratum-ibid. **B304**, 921 (1988).

[23] A. Denner, S. Dittmaier, M. Roth, D. Wackeroth, *Nucl. Phys.* **B560**, 33 (1999).

[24] W. Kilian, LC-TOOL-2001-039, 2nd ECFA/DESY Study 1998-2001, p. 1924.

[25] T. Stelzer, W.F. Long, *Comput. Phys. Commun.* **81**, 357 (1994).

[26] M. Beccaria, S. Prelovsek, F.M. Renard, C. Verzegnassi, *Phys. Rev.* **D64**, 053016 (2001).

[27] M. Beccaria, F.M. Renard, C. Verzegnassi, `hep-ph/0212247`.

[28] M. Beccaria, F.M. Renard, C. Verzegnassi, *Phys. Rev.* **D69**, 113004 (2004).

[29] M. Beccaria, F.M. Renard, C. Verzegnassi, `hep-ph/0405036`.

[30] F. del Aguila, J.A. Aguilar-Saavedra, *Phys. Rev.* **D67**, 014009 (2003).

[31] T. Stelzer, Z. Sullivan, S. Willenbrock, *Phys. Rev.* **D58**, 094021 (1998).

[32] B. Lampe, *Nucl. Phys.* **B454**, 506 (1995).

[33] E. Boos, L. Dudko, T. Ohl, *Eur. Phys. J.* **C11**, 473 (1999).

[34] S. Bejar, J. Guasch, J. Sola, *Nucl. Phys.* **B600**, 21 (2001).

[35] S. Bejar, J. Guasch, J. Sola, `hep-ph/0101294`.

[36] J.A. Aguilar-Saavedra, T. Riemann, `hep-ph/0102197`.

[37] J.A. Aguilar-Saavedra, `hep-ph/0409342`.

[38] S. Bejar, J. Guasch, J. Sola, *Nucl. Phys.* **B675**, 270 (2003).

[39] J. Guasch, J. Sola, *Nucl. Phys.* **B562**, 3 (1999).

[40] J.J. Liu, C.S. Li, L.L. Yang, L. G. Jin, `hep-ph/0406155`.

[41] J.J. Liu, C.S. Li, L.L. Yang, L. G. Jin, `hep-ph/0404099`.

[42] J.A. Aguilar-Saavedra, *Phys. Lett.* **B502**, 115 (2001).

[43] G. Eilam, J.L. Hewett, A. Soni, *Phys. Rev.* **D44**, 1473 (1991).

[44] E. Murayama, I. Watanabe, K. Hagiwara, KEK report 91-11, January 1992.

[45] S. Heinemeyer, S. Kraml, W. Porod, G. Weiglein, *J. High Energy Phys.* **0309**, 075 (2003).

[46] S. Heinemeyer, S. Kraml, W. Porod, G. Weiglein, `hep-ph/0409063`.

[47] P. Azzi *et al.*, `hep-ex/0404010`.

[48] V.M. Abazov *et al.*, *Nature* **429**, 638 (2004).

[49] A. Hoang *et al.*, *Eur. Phys. J.* **C3**, 1 (2000).

[50] M. Grünewald, `hep-ex/0304023`; updated as:
F. Teubert, talk given at "ICHEP04", Beijing, China, August 2004, see: `ichep04.ihep.ac.cn/data/ichep04/ppt/plenary/p21-teubert-f.ppt`; see also: `lepewwg.web.cern.ch/LEPEWWG/Welcome.html`.

[51] U. Baur, R. Clare, J. Erler, S. Heinemeyer, D. Wackeroth, G. Weiglein, D. Wood, `hep-ph/0111314`.

[52] M. Awramik, M. Czakon, A. Freitas, G. Weiglein, *Phys. Rev.* **D69**, 053006 (2004).

[53] M. Awramik, M. Czakon, A. Freitas, G. Weiglein, `hep-ph/0407317`, to be published in *Phys. Rev. Lett*; M. Awramik, M. Czakon, A. Freitas, G. Weiglein, `hep-ph/0408207`; M. Awramik, M. Czakon, A. Freitas, G. Weiglein, `hep-ph/0409142`.

[54] A. Freitas, W. Hollik, W. Walter, G. Weiglein, *Phys. Lett.* **B495**, 338 (2000); *Nucl. Phys.* **B632**, 189 (2002); M. Awramik, M. Czakon, *Phys. Rev. Lett.* **89**, 241801 (2002); A. Onishchenko, O. Veretin, *Phys. Lett.* **B551**, 111 (2003); M. Awramik, M. Czakon, A. Onishchenko, O. Veretin, *Phys. Rev.* **D68**, 053004 (2003); M. Awramik, M. Czakon, *Phys. Lett.* **B568**, 48 (2003).

[55] G. Degrassi, P. Gambino, A. Sirlin, *Phys. Lett.* **B394**, 188 (1997).

[56] M. Faisst, J. Kühn, T. Seidensticker, O. Veretin, *Nucl. Phys.* **B665**, 649 (2003).

[57] A. Freitas, S. Heinemeyer, G. Weiglein, *Nucl. Phys. Proc. Suppl.* **116**, 331 (2003).

[58] R. Barate *et al.*, *Phys. Lett.* **B565**, 61 (2003).

[59] S. Heinemeyer, G. Weiglein, *J. High Energy Phys.* **0210**, 072 (2002).

[60] R. Barbieri, M. Beccaria, P. Ciafaloni, G. Curci, A. Vicere, *Nucl. Phys.* **B409**, 105 (1993); J. Fleischer, F. Jegerlehner, O.V. Tarasov, *Phys. Lett.* **B319**, 249 (1993).

[61] M. Martinez, R. Miquel, *Eur. Phys. J.* **C27**, 49 (2003).

[62] B. Allanach *et al.*, *Eur. Phys. J.* **C25**, 113 (2002).

[63] G. Weiglein, *Nature* **429**, 613 (2004).

[64] M. Carena, S. Heinemeyer, C. Wagner, G. Weiglein, `hep-ph/9912223`; *Eur. Phys. J.* **C26**, 601 (2003).

[65] G. Degrassi, S. Heinemeyer, W. Hollik, P. Slavich, G. Weiglein, *Eur. Phys. J.* **C28**, 133 (2003).

[66] M. Krawczyk *et al.*, *Acta Phys. Pol. B* **35**, 2633 (2004), these proceedings.

[67] A. Denner *et al.*, *Acta Phys. Pol. B* **35**, (2004).

[68] W. Beenakker, S. Dittmaier, M. Kramer, B. Plumper, M. Spira, P.M. Zerwas, *Nucl. Phys.* **B653**, 151 (2003).

[69] W. Beenakker, S. Dittmaier, M. Kramer, B. Plumper, M. Spira, P.M. Zerwas, *Phys. Rev. Lett.* **87**, 201805 (2001).

[70] W. Bernreuther, R. Bonciani, T. Gehrmann, R. Heinesch, T. Leineweber, P. Mastrolia, E. Remiddi, `hep-ph/0406046`.

[71] M. Beneke, A.P. Chapovsky, A. Signer, G. Zanderighi, *Phys. Rev. Lett.* **93**, 011602 (2004).

[72] M. Beneke, A.P. Chapovsky, A. Signer, G. Zanderighi, *Nucl. Phys.* **B686**, 205 (2004).